Title

Transverse spatiotemporal variability of lowland river properties and effects on metabolic rate estimates

Journal

Water Resources Research, 50(1)

ISSN

1944-7973

Authors

Villamizar, Sandra R
Pai, Henry
Butler, Christopher A
et al.

Publication Date

2014

DOI

10.1002/2013WR014245

Peer reviewed

Transverse spatio-temporal variability of lowland river properties and effects on metabolic rates estimates

Sandra R. Villamizar*, Henry Pai, Christopher A. Butler, and Thomas C. Harmon

Environmental Systems Program & Sierra Nevada Research Institute
University of California, Merced

Final version published in

Water Resources Research

January, 2014

***Corresponding author:**
Sandra R. Villamizar
School of Engineering
University of California, Merced
5200 North Lake Road
Merced, CA 95343
svillamizar_amaya@ucmerced.edu
(209) 349-1521

Abstract

Variability of river properties such as temperature, velocity, dissolved oxygen (DO) and light at small scales (centimeters to meters) can play an important part in determining ecosystem structure and function. We hypothesize that significant transverse cross-sectional DO variation is observable within a river. Such variation may influence conventional single-station metabolic rate (primary production and respiration) estimates with respect to DO probe location, and reveal important connections between physical and biogeochemical processes and their drivers in rivers. . Using a mobile sensor system, we measured river properties across a bend in the lower Merced River in Central California under stationary flow conditions in April and September. Cross-sectional temperature, DO and chlorophyll-*a* concentrations exhibited modest but significant gradients which varied in magnitude and direction on a diel basis. The spatiotemporal variation was consistent with reach geomorphology and incident light patterns. Gross primary production (*GPP*), community respiration (CR_{24}) and net ecosystem production (*NEP*) rates estimates derived from local DO and temperature time series varied by 3 to 10% over the river cross-section, with greater variation in late summer. The presence of transverse metabolic rate gradients in this relatively simple reach implies the existence of substantial gradients in more complex river regimes, such as those spanning distinctively different microhabitats, transient storage zones and related distributed biogeochemical zones.

1. Introduction

Small-scale spatial variability (centimeters to meters) of river properties such as temperature, velocity, dissolved oxygen (DO) and light, plays an important role in determining local ecosystem structure and function [*Brooks et al.,* 2005; *Reid et al.,* 2006]. This physicochemical variability results in microhabitats affecting and being affected by aquatic plants and benthic algae [*Biggs,* 1996; *Biggs et al.,* 1998], invertebrates [*Brooks et al.,* 2005] and fish [*Finstad et al.,* 2007]. In this work, we examine small-scale spatiotemporal variation in river temperature and dissolved oxygen, as well as ecosystem metabolism estimates (primary production and respiration) derived from these observations.

Metabolism metrics derived from DO cycling behavior, such as gross primary production (*GPP*), ecosystem respiration (CR_{24}), and net ecosystem production (*NEP*, where $NEP = GPP - CR_{24}$) have long been used to characterize aquatic ecosystem dynamics [*Odum,* 1956; *Mulholland et al.,* 2001]. *GPP*, CR_{24} and *NEP* (referred to as stream metabolism or metabolic rates) are typically estimated as reach-averaged values using the single or two-station open water method based on diel DO and water temperature observations [*Odum,* 1956; *McCutchan Jr. et al.,* 1998; *Mulholland et al.,* 2001; *McCutchan Jr. et al.,* 2002; *Hall Jr. and Tank,* 2005]. These methods assume that the stream is well mixed in the vertical and transverse dimensions. Here, we test the assumption of complete transverse mixing by examining DO cycling and metabolism estimates locally over small scales.

The occurrence and drivers of spatial heterogeneity of metabolic rates have been investigated in lakes [*Van de Bogert et al.,* 2007]. In some cases metabolism drivers are

clear. For example, we know that lakes tend to stratify by temperature, leading to vertical DO, light, nutrient and biomass gradients, and that productivity decreases with depth. However, it is unclear why lake respiration appears to be unaffected by depth [*Coloso et al.,* 2008]. In another example, seasonally averaged metabolic drivers have been linked to total phosphorous and dissolved organic carbon levels [*Hanson et al.*, 2003; *Sand-Jensen and Staehr,* 2007]. However, driver identification over shorter time-scales remains an elusive goal due to the spatio-temporal heterogeneity of the potential drivers [*Coloso et al.,* 2011]. The shorter-term heterogeneities result from wind conditions relative to site-specific morphologic features and the lake's spatial complexity, including the division between the open water (pelagic) and the benthically-influenced littoral zone [*Van de Bogert et al.,* 2007; *Vadeboncoeur et al.,* 2008; *Van de Bogert et al.,* 2012].

River ecosystems exhibit DO patterns similar to those of lakes, suggesting that some findings about net *NEP* in lakes may be relevant to rivers. Like lakes, rivers exhibit spatially heterogeneous DO and temperature distributions in spite of their state of continual mixing (relative to lakes). Longitudinal changes in the metabolism within a river, and differences between rivers, are driven by temperature, nutrient loading, and light availability (e.g., [*Hoellein et al.,* 2007; *Von Schiller et al.,* 2008; *Griffiths et al.,* 2013]). Vertical mixing in rivers is rapid compared to longitudinal mixing, yet vertical gradients in DO, temperature and nutrients are observable [*Lorke et al.,* 2012; *Berg et al.,* 2013]. Transverse mixing timescales for rivers are intermediate to those for longitudinal and vertical mixing for a given river [*Fisher et al.,* 1979; *Rutherford,* 1994]. More recent studies underscore the importance of transverse heterogeneity of biogeochemical constituents due to exchange processes between the main channel and transient storage

zones [*Ensign and Doyle,* 2005; *Gooseff et al.,* 2011] and/or the hyporheic zone [*Haggerty et al.,* 2002; *Bencala,* 2005; *Cardenas et al.,* 2008]. These exchange processes, along with morphology- and light-related spatial distributions of pelagic and the benthic communities (as noted above for lakes), support the existence of small-scale variability of riverine metabolic rates.

In this work we employ a high-frequency spatiotemporal monitoring approach to study small-scale spatial variations in cross-sectional river temperature, DO, and light. We estimate local metabolic rate parameters using local times series data generated at the multiple monitoring stations. Our goals are to (1) identify spatial trends in temperature, DO, chlorophyll-*a* (as a proxy for biomass), and light, and (2) connect those trends to small-scale variation in river metabolism estimates.

2. Methods

To assess transverse spatial-temporal variation in river DO, temperature and metabolic rate estimates, we deployed two multi-parameter water quality sensors in a cross-section of a partially shaded reach of the Lower Merced River (section 2.1). One sensor was the stationary control and collected data continuously following the conventional single-station approach [*Odum,* 1956; *Mulholland et al.,* 2001]. We simultaneously deployed a mobile sensor to scan the DO, temperature, and chlorophyll-*a* spatial distributions repetitively over the cross-section. We also monitored light availability at several locations across the same transect. We analyzed the observed distributed water quality properties, local velocities and light conditions to identify spatial patterns (section 2.2). Then, we assessed daily metabolic rate parameters (*GPP*, CR_{24},

and *NEP*) using local DO and temperature time series data from the mobile sensor (section 2.3).

2.1. Site Description and Experimental Setup

The study site is located at river km 26 of the lower Merced River, an agriculturally dominated, impounded river in Central California (Figure 1). We conducted sampling campaigns in April and September under base flow conditions, before and after irrigation season, respectively. For these time periods, the study reach was a single-thread meandering river with a narrow channel width ranging between 20 and 40 meters. The reach-averaged slope was 0.0003 and the bed sediment was predominantly sand [*Stillwater Sciences*, 2002]. At the time of the study, patches of large woody debris were present in upstream areas of the study reach, creating localized low velocity zones on the left side and forcing the channel to the right (downstream view). We installed the experimental setup (described below) downstream of the debris, at a bend, where the main channel crossed over to the left side. The bar (right) side of the transect and upstream segment hosted a macrophyte stand which provided observable resistance to flow within 1 to 2 m of the right bank. The riparian canopy on the right side was relatively open. The river thalweg on the left was bounded by a riparian zone characterized by riprap revetment and approximately one tree-width of native vegetation. Given the reach orientation (Figure 1) the canopy (roughly 7-10 m in height) shaded the left side of the river from dawn to late afternoon during the experiments.

Figure 1. Satellite image of the Merced River study reach (source: Google Earth).

Under spring (April 20-25) and late summer (September 7-12) 2009 baseflow conditions, we deployed the stationary and mobile monitoring systems to test for

158 spatiotemporal variation of DO and temperature. We installed a multi-parameter sonde
159 (Hach Hydrolab Model DS5) near the center of the river, 9.5 m from the right bank
160 (Figure 2). With this sonde (the fixed station), we continuously monitored water
161 temperature (Temp, ±0.01 °C), luminescent dissolved oxygen (DO, ±0.01 mg L^{-1}), and
162 photosynthetically active radiation (PAR, ±1 µmol m^{-2} s^{-1}). Two meters upstream of the
163 fixed station, we deployed a tethered robotic sensor platform [*Harmon et al.*, 2007] (the
164 mobile station) to monitor the transverse spatial distribution of local velocity (Sontek
165 ADV, Vel, ±0.0001 m s^{-1}) and water quality using a similar multi-parameter sonde (Hach
166 Hydrolab Model DS5) that collected water temperature (Temp, ±0.01 °C), luminescent
167 dissolved oxygen (DO, ±0.01 mg L^{-1}) and Chlorophyll-*a* by means of a fluorescence
168 sensor (Chl, ±0.01 µg L^{-1}, Turner Design). All the water-quality sensors were previously
169 calibrated according to vendor specifications, but the DO sensor responses were more
170 extensively characterized (see below).

171 The mobile station initiated each robotic scan at position x = 1.5 m from the right
172 bank of the river (point 1) because locations closer than 1.5 m were too shallow to
173 provide adequate probe clearance. The scan continued along the transect sampling at two-
174 meter intervals until reaching the left bank (with the exception of the final point which
175 was only 1 m from the prior location). The system performed repetitive scans, dwelling
176 for 60 s at each sampling point. The data collection strategy for the fixed and mobile
177 systems is summarized in (Table 1). Occasional nighttime power depletion interrupted
178 the robotic sampling routine, necessitating data gap-filling (see below). We estimated
179 metabolic rate parameters by integrating DO observations over 24-hour cycles (section
180 2.3). Thus, the 93 and 114 raster scans completed during the spring and late summer

experiments yielded spatiotemporal metabolic rate estimates for three and four diel cycles, respectively.

We monitored local light availability across the experimental transect to support the interpretation of the metabolic estimates. We placed three self-logging sensors (5-min intervals, Hobo Temp/Light Pendants, Onset Computer) sampling temperature (±0.10 °C) and irradiance (0 to 320,000 lux), at three distances from the right bank in fully exposed, partially shaded and fully shaded areas (L-1, -2, and -3, respectively, Figure 2). We monitored local meteorological conditions using a weather station (Davis Wireless Vantage Pro2™) positioned 1 m above the river surface, recording air temperature (±0.1 °C), solar radiation (±1 W m^{-2}), and other parameters. We obtained open-canopy solar radiation conditions from a California Irrigation Management Information System (CIMIS) station located 18 km southwest of the experimental site.

Figure 2. Photograph of the experimental set up. (A) mobile sampling unit (water quality and velocity); (B) fixed sampling unit (water quality and PAR); (WS) weather station; (L-1, L-2, L-3) light intensity sensors. The image captures the predominant shading pattern along the left bank of the river.

Table 1. Summary of the sampling plans for the fixed and mobile systems.

In order to establish the signal-to-noise ratio for our cross-sectional analysis, we characterized the DO sensors relative to one another and with respect to potential signal drift. In a controlled laboratory set up, we confirmed the factory-reported precision of ±0.01 mg L^{-1}. The two sensors exhibited an absolute difference of 0.03±0.04 (±2 SD) mg L^{-1}. No DO signal drift occurred for either sensor in an experiment spanning 7 days. For each scan by the mobile sensor, we used the ratio of the cross-sectional coefficient of variation (CV_{exp}, the ratio of the standard deviation to the mean value of the readings for a

given raster scan) to that of the DO sensor (CV_{std}, the ratio of the sensor's standard deviation under controlled conditions (±0.01 mg L^{-1}) to the mean sensor reading) to identify meaningful spatial DO variations. In doing so, we assumed that temporal changes in DO and temperature over one spatial sampling cycle were negligible (approximately 20 min per scan).

We used a spline interpolation scheme to fill the aforementioned DO and temperature data gaps at a 1-min interval for each of the sampling positions. The plots in (Figure 3) demonstrate the consistency in the temporal trends for the high resolution single-station data and the interpolated data from nearby stations within the transect, verifying that the interpolation scheme did not bias the gap-filled data. One exception was noted for the latter part of the April time series, where the data loss happened near the minimum of the DO curve. In this case, the interpolation was deemed unreliable and the data set was truncated at midnight April 25.

Figure 3. Example of the interpolation scheme for dissolved oxygen (top) and water temperature (bottom) for the April data set. The continuous (grey) line represents the fixed-station data used for comparison, and the symbols and black line represent the observations and 1-min spline-interpolation, respectively, for the nearest sampling point (x = 9.5 m) of the distributed data set.

2.2. Spatial Analysis

We calculated the spatial autocorrelation statistic (global Moran's *I*) to test for statistically significant spatial patterns in the cross-sectional water quality observations, [*Moran*, 1950]. The *I* statistic is calculated as

$$I = \frac{n}{\sum_{i=1}^{i=n}\sum_{j=1}^{j=n} W_{ij}} \frac{\sum_{i=1}^{i=n}\sum_{j=1}^{j=n} W_{ij}\left(x_i - \bar{x}\right)\left(x_j - \bar{x}\right)}{\sum_{i=1}^{i=n}\left(x_i - \bar{x}\right)^2} \quad \textbf{(1)}$$

where n is the number of spatially distributed observations, W_{ij} is the spatial weight matrix, x_i and x_j are the values of variable x at positions i and j, and $\bar{x}$ is the mean value of the spatially distributed observations. The inter-locality weights W_{ij} used in the spatial weight matrix are the inverse of the square of the spatial separation between the sampling points [*Wartenberg*, 1985].

For the I statistic, the null hypothesis states that there is no spatial clustering, i.e., there is a random spatial distribution of the parameter values in a given study area ($I \approx 0$); I values approaching 1 suggest a clustered organization of the parameter of interest; and I values approaching -1 describe a perfectly dispersed pattern. To test for the significance of I, we calculate T based on the Randomization Null Hypothesis [*Cliff and Ord*, 1973]

$$T = \frac{\left(I - E\left[I\right]\right)}{\sqrt{Var(I)}} \quad \textbf{(2)}$$

where T is the t-score because of our relatively small number of sampling points, $E[I]$ is the expected value of I under the null hypothesis of no spatial autocorrelation

$$E\left[I\right] = \frac{-1}{n-1} \quad \textbf{(3)}$$

and $Var[I]$ is the variance, calculated as

$$Var\left[I\right] = E[I^2] - E[I]^2 \quad \textbf{(4)}$$

The calculation of $E[I^2]$ is explained elsewhere [*Cliff and Ord*, 1973].

2.3. Whole-Stream Metabolism Estimation

To link the cross-sectional DO and temperature observations to ecosystem metabolism, we estimated daily GPP, CR_{24} and NEP, at each sampling station. We used the single-

248 station approach [*Bott,* 2007]. The single-station method assumes that a point
249 measurement reflects a cross-sectional average of DO conditions developed over a
250 relatively homogeneous upstream reach. The intent here is to test that assumption by
251 applying the method to an array of single-stations a cross-section.In the single-station
252 method, the instantaneous change of DO is modeled as

253 $$\frac{dC}{dt} = p(t) - r + K_2(C_s - C) \quad \textbf{(5)}$$

254 where C is the DO concentration [ML^{-3}], $p(t)$ is the time-variant rate of primary
255 production [$ML^{-3}T^{-1}$], r is the community respiration rate [$ML^{-3}T^{-1}$], and the last term
256 describes stream reaeration in terms of K_2, the reaeration rate constant [T^{-1}], and (C_s - C),
257 the DO deficit [ML^{-3}], where C_s [ML^{-3}] is the DO saturation value at the current
258 temperature. Whole-stream metabolism is then estimated by integrating **(5)** over a 24-h
259 period, as described below, to yield a daily DO balance

260 $$Q_{24} = GPP - CR_{24} + D \quad \textbf{(6)}$$

261 where Q_{24}, the 24-h net rate of change of DO, is a function of the average daily gross
262 primary production (GPP), community respiration (CR_{24}) and stream reaeration rates (D)
263 [$ML^{-3}T^{-1}$]. Equation (**5**) can be modified to account for groundwater input which can
264 affect DO levels and hence metabolism estimates [*McCutchan Jr. et al.,* 2002; *Hall Jr.*
265 *and Tank,* 2005]. For the river stage and location of this study, we estimated that
266 groundwater discharge constituted less than one percent of the overall flow [*Zamora,*
267 2007; *Butler,* 2009] and therefore neglected this input.

We estimated daily *GPP* values by integrating the observed DO change (*dC/dt*) over each diel cycle, while adjusting for the temperature-corrected photoperiod respiration rate (r_T) and reaeration coefficient ($K_{2,T}$):

$$GPP = \int_{\phi} \left(\frac{dC}{dt} - K_{2,T}\left(C_s - C\right) + r_T \right) dt; \quad \phi = photoperiod \qquad \textbf{(7)}$$

Similarly, we obtained daily community respiration rate (CR_{24}) by integrating the instantaneous temperature-corrected respiration rates over the 24-h period:

$$CR_{24} = \int_{24\,h} r_T \; dt \qquad \textbf{(8)}$$

For equations **(7)** and **(8)**, the instantaneous respiration rate (r_T) is an average of the reaeration-corrected rates of DO change during dark hours [*Marzolf et al.,* 1994], corrected for the diel temperature variations as [*Erlandsen and Thyssen,* 1983]

$$r_T = r_{20}\,\theta_r^{(T-20)}, \quad \theta_r = 1.07 \qquad \textbf{(9)}$$

Among the various methods for estimating stream reaeration [*Covar,* 1976; *Wilcock,* 1982; *Thyssen et al.,* 1987; *Genereux and Hemond,* 1992; *McBride,* 2002; *Aristegi et al.,* 2009], we selected the energy dissipation model EDM [*Tsivoglou and Neal,* 1976]. This method has been found to be reliable in comparison with results from tracer studies [*Wilcock,* 1988] and offered low mathematical uncertainty for the calculation of the reaeration rates. The EDM uses the reach-averaged properties to calculate a single value

$$K_{2,20} = K'\,S\,U \qquad \textbf{(10)}$$

where $K_{2,20}$ (d^{-1}) is the reaeration rate constant at 20°C, *K'* is 15300 s m^{-1} d^{-1} for flows above 0.56 m^3 s^{-1} [*Hein,* 2005], *S* is the reach slope (m m^{-1}), and *U* is the mean reach

velocity (m s^{-1}). This daily rate ($K_{2,20}$) was applied at both the stationary and the distributed sampling locations with the appropriate correction for temperature variations [*Elmore and West*, 1961]

$$K_{2,T} = K_{2,20}\,\theta_K^{(T-20)}, \quad \theta_K = 1.0241 \qquad \textbf{(11)}$$

Lastly, we used the *GPP* and CR_{24} estimates to calculate net ecosystem productivity ($NEP=GPP-CR_{24}$), which is used to evaluate the overall functioning of the ecosystem. Positive or negative *NEP* values indicate the autotrophic or heterotrophic character of the system, respectively. These rates may be expressed in either areal (g O_2 m^{-2} day^{-1}) or volumetric units (g O_2 m^{-3} day^{-1}).

3. Results and Discussion

3.1. Site Conditions during the Experiment Periods

Flow stationarity was verified by the reasonably constant cross-sectional velocity distributions during each of the two study periods (Figure 4). Mean daily flow and water temperature during the April and September periods were 6 m^3 s^{-1}, 21 °C and 3.7 m^3 s^{-1}, 23 °C, respectively. The lower flows correspond with slightly lower velocities during September (5 to 50 cm s^{-1}) compared to April (5 to 60 cm s^{-1}). For both experiments, the lowest velocities occurred, as expected, near the river banks. Bed movement during the interceding period is evident from the cross-sectional bed elevation lines.

Figure 4. Profiles of daily-average velocities across the river transect during April (top) and September (bottom). Dashed lines with symbols represent velocities for day 1 (diamonds – September only), day 2 (black circles), day 3 (triangles), and day 4 (squares). The gray circles indicate the position of the sampling points for the distributed system [vertical scale exaggerated].

The weather conditions were less stable during the April time period (Figure 5). Sampling days 1 and 2 were characterized by warm days and cool nights followed by a

change in regional weather with marked effects on days 3 and 4, as reflected by the temperature (Figure 5a) and solar radiation data (Figure 5b-c). In September, more stable conditions with warmer temperatures relative to April occurred for all four days. Times for maximum and minimum air temperatures were similar for both periods (5 pm and 6:30-7:00 am, respectively) and the days were about 40 to 60 min longer during the April experiment. The incident maximum solar radiation values occurred between noon and 1 pm for both periods, reaching 900 W m^{-2} in April and 850 W m^{-2} in September (Figure 5b-c). The influence of cloud cover was evident on days 1 and 4 in April, and on day 4 in September, based on the open-canopy radiation data (Figure 5c).

Figure 5. Time series of (a) air temperature, (b) on-site solar radiation, and (c) open-canopy radiation (CIMIS weather station) (black line: April data; grey line: September data).

The normalized light intensity data was representative of the light conditions upstream of the experimental cross-section (Figure 6). In general, the left, deeper side of the reach received 10-20% of the incident light received at the right side (daily average) due to the shading pattern produced by the northeast to southwest reach orientation and the riparian vegetation structure. The exception was the morning of April 24, when the cloudy conditions produced a more diffuse pattern resulting in an increase to 50% of the daily average incident light reaching the left side with respect to that of the right side.

Figure 6. Incident light patterns represented by the normalized light intensity for three different positions across the river transect. (Top: April 21-24; bottom: September 08-11). The observations (lux) were normalized by the maximum observed value for the two experiments (200,000 lux).

3.2. Transverse Water Quality Gradients

In this section, we present and validate the hypothesized transverse gradients in water quality properties, and discuss their causes. The comprehensive water quality data set

(Figure 7) demonstrated the expected diel cycling of water temperature, DO, and chlorophyll-*a*. In general, the river was cooler with higher DO concentrations in April, and the warmer and slower water of September appeared to support a greater standing phytoplankton biomass, based on the chlorophyll-*a* data. Careful inspection of the individual transect sampling events of (Figure 7) suggested the presence of transverse gradients (Figure 8).

Figure 7. Temperature (Temp), dissolved oxygen (DO) and chlorophyll-*a* (Chl), spatiotemporal behavior observed using the mobile sensor platform. For each panel, the horizontal axis represents position within a raster scan from the right to the left river bank (downstream view), the vertical axis represents the average sampling time for each raster scan (intervals are non-uniform in time), and the colored cells represent the value of each sampled parameter (DO, Temp, Chl) for the corresponding position and time (note differences in scale).

We use the Moran's *I* test to confirm the existence of significant cross-sectional spatial clustering (hereafter referred to as gradients) of temperature, DO and chlorophyll-*a* observations (Figure 8). The emergence and dispersal of significant gradients (*I* approaching 1.0) exhibited diel patterns. Significant temperature gradients occurred for most of the sampling events during the day and at night (Figure 8a). Gradients consistently dissipated for a brief period in the early afternoon. Similar to temperature, DO gradients emerged during the day and dissipated overnight (Figure 8b) as expected from diurnal photosynthetic processes. These gradients also dissipated in the early afternoon suggesting a connection to the temperature gradient change. Significant chlorophyll-*a* gradients in September (Figure 8c) mainly coincided with those for DO. April chlorophyll-*a* observations generally exhibited similar but slightly stronger gradients. Neither the April nor the September chlorophyll-*a* observations exhibited the consistent midday gradient dispersal that was prominent in the temperature and DO data.

Figure 8. Time series of the calculated Moran's *I* statistic for the two experiment periods. Black symbols refer to the April results and grey symbols to those of September. The filled dots indicate the transect runs with significant gradients ($p<0.05$; for April: 81 (Temp), 67 (DO), and 62 (Chl) out of 90 transect runs; for September: 100 (DO), 77 (Temp), and 54 (Chl) out of 105 transect runs).

For DO, the temporal trends of the coefficient of variation ratio (CV_{exp}/CV_{std}) (Figure 9) clarified the diel patterns suggested by the Moran's *I* statistic (Figure 8). Overall, variability over the sampling transect was greater in September, which is consistent with the greater chlorophyll-*a* concentrations of that period (using chlorophyll-*a* as a proxy for biomass concentrations). Cross-sectional DO variation peaked in late morning and late afternoon for both experiments. The April ratios ranged from about 2 to 6, and their temporal trend was repeated for days 1 through 3. The trend was less noticeable during day 4, likely due to the different weather conditions (lower temperatures and incident radiation) of that day. *CV* ratios for September ranged from 2 to 12. One anomalously high CV ratio occurred for unknown reasons around 18:00 on the third day of the September sampling period. Otherwise, a second rise of CV ratios occurred in the late afternoon similar in magnitude but earlier relative to the April results. The two apparent peaks in the CV ratio for DO were likely indicative of daily productivity with the midday pattern dissipation caused by the temperature gradient reversal, as suggested in the context of the Moran's I results above.

Figure 9. Time series for April (top) and September (bottom) of normalized coefficients of variation (*CV*) for spatially distributed DO concentrations at the times shown (each symbol represents the variability of one croo-sectional sampling event).

Daytime cross-sectional raster scans of temperature, DO and chlorophyll-*a* were selected to demonstrate the representative gradient changes that occurred each day (Figure 10). Transverse temperature variability (Figure 10a) was consistent with river

390 reach geomorphology and orientation with respect to incident radiation (Figures 1 and 6).
391 Morning temperatures were cooler in the main channel (left side) relative to the bar
392 (right) side. In the afternoon, the temperature gradient was reversed as the main channel
393 side became warmer. The afternoon reversal was likely driven by the primary channel
394 which transitioned from the sunnier (right) side of the reach to the left side as it entered
395 the sampling transect (Figure 1). During the daytime, secondary flow in the bend would
396 have also contributed to the gradient reversal by conveying warmer water from the slow
397 moving, sunny bar (right) to the channel (left). For April, and to a lesser extent
398 September, the right-most sampling point exhibited markedly greater temperatures
399 compared to adjacent points. The higher incident radiation upon the shallow, slow-
400 moving water within the previously noted macrophyte stand on this side probably caused
401 this localized temperature increase.

402 The DO gradients were more definite in September, probably due to a larger
403 phytoplankton population during this time (Figure 10b). The steepest DO gradients
404 occurred in the morning hours with higher DO values towards the main channel and
405 decreasing to the right (shallow) side. The behavior of the right-most sampling point
406 during April (and to a lesser extent, September) is marked by an increase of the observed
407 DO concentrations during the day. As with temperature, increased DO levels at this
408 location appeared to have been the result of the macrophyte stand since macrophytes
409 exert considerable influence on water quality by modifying local flow patterns and DO
410 dynamics [*Wilcock et al.,* 1999; *Desmet et al.,* 2011].

411 Daytime chlorophyll-*a* gradients for April and September were similar to those for
412 DO, with concentrations higher in the main channel (left) and lower near the right bank

(Figure 10c). Variability was greater for the September period. In contrast to the DO data, locally elevated chlorophyll-*a* concentrations did not occur near the right bank. This discrepancy suggests that the aforementioned macrophyte stand may have enhanced temperature and DO concentrations, but did not affect local chlorophyll-*a* concentrations.

Figure 10. Deviation of local (a) temperature, (b) DO and (c) chlorophyll-*a* measurements from the cross-sectional average for selected morning and afternoon sampling events in April (left) and September (right).

3.3. Implications of the Observed Transverse Gradients on the Distributed Metabolic Rate Estimates

Spatial distributions for the metabolic rate estimates exhibited modest but discernible gradients over the experimental transect (Figure 11). This finding is not surprising given the aforementioned variability in the spatiotemporal DO distributions underlying these metabolism calculations (see Figure 9 and Figure 10). To better visualize the patterns, the distributed daily metabolic rates were normalized by the estimates obtained at the thalweg, point 10 (Figure 4), for their respective day. For reference, (Table 2) presents the reach-averaged metabolic rate estimates based on the fixed station observations which are in agreement with other studies developed for lowland, heterotrophic rivers [*Wilcock et al.*, 1998; *Oliver and Merrick*, 2006].

Table 2. Areal metabolic rate estimates based on DO and temperature observations from the fixed setup using average reach velocity and depth (the error bars are based on propagation of velocity and depth uncertainty through the reaeration and metabolism calculations).

Driven by the daily cycling of DO (Figure 9), *GPP* estimates exhibited more variation in September than in April (Figure 11a). April *GPP* values increased slightly from left to right, changing by less than about 3% over the cross-section (Figure 11a, left). In contrast, the September *GPP* distributions varied in a non-monotonic manner, and

changed by 5% to 10% over the cross-section, depending on the specific date (Figure 11a, right). An approximate estimate of the transverse mixing length [*Fisher et al.*, 1979] based on the average properties of the study reach suggests transverse mixing time scales on the order of 1 to 4 hours. Because of the physiological responses of phytoplankton to changes in light intensity and temperature occur at different time scales, ranging from minutes to a few hours [*Falkowski*, 1984; *Neale and Marra*, 1985; *Pahl-Wostl and Imboden*, 1990; *MacIntyre et al.*, 2000], it is likely that these gradients in metabolic rate estimates were real, the result of contrasting mixing and biological processes time scales.

Like *GPP*, the respiration rate estimates are based on DO variation and similar trends happened for the normalized distribution of CR_{24} (Figure 11b). The resulting *NEP* estimates (the difference of *GPP* and CR_{24}) were consistent for the two sampling periods, and varied by about 20% over the cross-section, generally increasing from left to right (more heterotrophic toward the right side). For April, the *NEP* variation was driven primarily by the respiration rates, while the September *NEP* variation was more of a function of both the production and respiration estimates (Figure 11c).

Figure 11. River cross-sectional distributions for (a) *GPP*, (b) CR_{24}, and (c) *NEP*, for April (left) and September (right). Values are normalized with respect to the estimates obtained at point 10 (thalweg position) of the sampling transect. Error bars are based on the propagation of velocity and depth uncertainty through the reaeration and metabolism calculations.

4. Summary and Conclusions

To assess the potential for small scale metabolic rate variability over a river cross-section, we examined the temperature and constituent concentrations (DO and chlorophyll-*a*). For DO, the primary variable for metabolism estimates, we observed gradients developing and dissipating daily in both April and September experiments, with

more prominent gradients being exhibited during September. The DO gradients consistently increased during morning hours, in accordance with incident light patterns and channel geometry within the upstream reach. The observed gradients of DO resulted in spatially distributed metabolic rate estimates, supporting our hypothesis of the existence of small-scale, transverse heterogeneities of these river ecosystem metrics.

For this experiment on a channelized river bend, the spatial variability in metabolism estimates was minor. In effect, location of a sampling station within a few meters of the thalweg would yield representative metabolism estimates for the river reach. Nevertheless, the presence of small scale gradients in metabolic rates in this relatively simple reach implies the existence of substantial gradients in geomorphically complex cross-sections, such as those with more distinctive microhabitats and/or transient storage zones. In this study, the observed contrast between the macrophyte stand environment and the main channel exemplified this point.

Lastly, it is important to note that although using DO as a proxy for metabolism is a well-established method, it is an indirect assessment. Hence, additional data pertaining to local nutrient cycling and direct biomass assessments are needed to better clarify the interrelation between hydrodynamic and metabolic processes and time scales.

Acknowledgments – This work was supported by the National Science Foundation (Awards CCF-0120778, and EAR-0854566), and by the Inter-American Institute for Global Change Research (IAI) CRN3038 (under US NSF Award GEO-1128040). We thank Patrick Barnes and Alex Rat'ko for their valuable support during the field campaigns.

References

Aristegi, L., O. Izagirre, and A. Elosegi (2009), Comparison of several methods to calculate reaeration in streams, and their effects on estimation of metabolism, *Hydrobiologia, 635*, 113-124.

Bencala, K. E. (2005), Hyporheic exchange flows, in *Encyclopedia of Hydrological Sciences*, edited by M. G. Anderson, pp. 1733-1740, John Wiley & Sons, Ltd.

Berg, P., M. H. Long, M. Huettel, J. E. Rheuban, K. J. McGlathery, R. W. Howarth, K. H. Foreman, A. E. Giblin, and R. Marino (2013), Eddy correlation measurements of oxygen fluxes in permeable sediments exposed to varying current flow and light, *Limnol. Oceanogr., 58*, 1329-1343.

Biggs, B. J. F. (1996), Hydraulic habitat of plants in streams, *Regulated Rivers-Research & Management, 12*, 131-144.

Biggs, B. J. F., D. G. Goring, and V. I. Nikora (1998), Subsidy and stress responses of stream periphyton to gradients in water velocity as a function of community growth form, *J. Phycol., 34*, 598-607.

Bott, T. L. (2007), Primary productivity and community respiration, in *Methods in Stream Ecology*, 2nd edn., edited by F. Richard Hauer and Gary A. Lamberti, pp. 663-690, Academic Press.

Brooks, A. J., T. Haeusler, I. Reinfelds, and S. Williams (2005), Hydraulic microhabitats and the distribution of macroinvertebrate assemblages in riffles, *Freshwat. Biol., 50*, 331-344.

Butler, C. A. (2009), A rapid method for measuring local groundwater-surface water interactions and identifying potential non-point source pollution inputs to rivers., 43.

Cardenas, M. B., J. L. Wilson, and R. Haggerty (2008), Residence time of bedform-driven hyporheic exchange, *Adv. Water Resour., 31*, 1382-1386.

Cliff, A. D. and J. K. Ord (1973), *Spatial Autocorrelation*, Monographs in Spatial and Environmental Systems Analysis, 178 pp., Pion Limited, London.

Coloso, J. J., J. J. Cole, P. C. Hanson, and M. L. Pace (2008), Depth-integrated, continuous estimates of metabolism in a clear-water lake, *Can. J. Fish. Aquat. Sci., 65*, 712-722.

Coloso, J. J., J. J. Cole, and M. L. Pace (2011), Difficulty in discerning drivers of lake ecosystem metabolism with high-frequency data, *Ecosystems, 14*, 935-948.

519 Covar, A. P. (1976), Selecting the proper reaeration coefficient for use in water quality
520 models, in *Proceedings of the Conference on Environmental Modeling and Simulation*,
521 vol. 600/9-76-016Anonymous , pp. 340-343, U.S. Environmental Protection Agency,
522 Cincinatti, Ohio.

523 Desmet, N. J. S., S. Van Belleghem, P. Seuntjens, T. J. Bouma, K. Buis, and P. Meire
524 (2011), Quantification of the impact of macrophytes on oxygen dynamics and nitrogen
525 retention in a vegetated lowland river, *Phys. Chem. Earth, 36*, 479-489.

526 Elmore, H. L. and W. F. West (1961), Effect of water temperature on stream reaeration,
527 *Journal of the Sanitary Engineering Division, 87*, 59-72.

528 Ensign, S. H. and M. W. Doyle (2005), In-channel transient storage and associated
529 nutrient retention: Evidence from experimental manipulations, *Limnol. Oceanogr., 50*,
530 1740-1751.

531 Erlandsen, M. and N. Thyssen (1983), Modelling the community oxygen production in
532 lowland streams dominated by submerged macrophytes, Analysis of Ecological Systems:
533 State-of-the-Art in Ecological Modelling, Fort Collins, CO, 24-28 May, 1982.

534 Falkowski, P. G. (1984), Physiological-responses of phytoplankton to natural light
535 regimes, *J. Plankton Res., 6*, 295-307.

536 Finstad, A. G., T. Forseth, O. Ugedal, and T. F. Naesje (2007), Metabolic rate, behaviour
537 and winter performance in juvenile Atlantic salmon, *Funct. Ecol., 21*, 905-912.

538 Fisher, H. B., E. J. List, R. C. Koh, J. Imberger, and N. H. Brooks (1979), Mixing in
539 rivers, in *Mixing in Inland and Coastal Waters*Anonymous , pp. 104-147, Academic
540 Press, Orlando, Florida.

541 Genereux, D. P. and H. F. Hemond (1992), Determination of gas-exchange rate constants
542 for a small stream on Walker Branch Watershed, Tennessee, *Water Resour. Res., 28*,
543 2365-2374.

544 Gooseff, M. N., D. A. Benson, M. A. Briggs, M. Weaver, W. Wollheim, B. Peterson, and
545 C. S. Hopkinson (2011), Residence time distributions in surface transient storage zones in
546 streams: Estimation via signal deconvolution, *Water Resour. Res., 47*, W05509.

547 Griffiths, N. A., J. L. Tank, T. V. Royer, S. S. Roley, E. J. Rosi-Marshall, M. R. Whiles,
548 J. J. Beaulieu, and L. T. Johnson (2013), Agricultural land use alters the seasonality and
549 magnitude of stream metabolism, *Limnol. Oceanogr., 58*, 1513-1529.

550 Haggerty, R., S. M. Wondzell, and M. A. Johnson (2002), Power-law residence time
551 distribution in the hyporheic zone of a 2nd-order mountain stream, *Geophys. Res. Lett., 29*, 1640.

553 Hall Jr., R. O. and J. L. Tank (2005), Correcting whole-stream estimates of metabolism
554 for groundwater input, *Limnology and Oceanography: Methods, 3*, 222-229.

555 Hanson, P. C., D. L. Bade, S. R. Carpenter, and T. K. Kratz (2003), Lake metabolism:
556 Relationships with dissolved organic carbon and phosphorus, *Limnol. Oceanogr., 48*,
557 1112-1119.

558 Harmon, T. C., R. F. Ambrose, R. M. Gilbert, J. C. Fisher, M. Stealey, and W. J. Kaiser
559 (2007), High-resolution river hydraulic and water quality characterization using rapidly
560 deployable networked infomechanical systems (NIMS RD), *EES, 24*(2), 151-159, doi:
561 10.1089/ees.2006.0033.

562 Hein, M. K. (2005), 10300 D. primary productivity, in *Standard Methods for the*
563 *Examination of Water & Wastewater*, 21st edn., edited by Andrew D. Eaton, Lenore S.
564 Clesceri, Eugene W. Rice, and Arnold E. Greenberg, pp. 10-37-10-45, APHA; AWWA;
565 WEF, Baltimore, Maryland, USA.

566 Hoellein, T. J., J. L. Tank, E. J. Rosi-Marshall, S. A. Entrekin, and G. A. Lamberti
567 (2007), Controls on spatial and temporal variation of nutrient uptake in three Michigan
568 headwater streams, *Limnol. Oceanogr., 52*, 1964-1977.

569 Lorke, A., D. F. McGinnis, A. Maeck, and H. Fischer (2012), Effect of ship locking on
570 sediment oxygen uptake in impounded rivers, *Water Resour. Res., 48*, W12514.

571 MacIntyre, H. L., T. M. Kana, and R. J. Geider (2000), The effect of water motion on
572 short-term rates of photosynthesis by marine phytoplankton, *Trends Plant Sci., 5*, 12-17.

573 Marzolf, E. R., P. J. Mulholland, and A. D. Steinman (1994), Improvements to the
574 diurnal upstream-downstream dissolved oxygen change technique for determining whole-
575 stream metabolism in small streams, *Canadian Journal of Fisheries and Aquatic*
576 *Sciences, 51*, 1591-1599.

577 McBride, G. B. (2002), Calculating stream reaeration coefficients from oxygen profiles,
578 *Journal of Environmental Engineering-Asce, 128*, 384-386.

579 McCutchan Jr., J. H., W. M. Lewis Jr., and J. F. Saunders III (1998), Uncertainty in the
580 estimation of stream metabolism from open-channel oxygen concentrations, *Journal of*
581 *the North American Benthological Society, 17*, 155-164.

582 McCutchan Jr., J. H., J. F. Saunders III, W. M. Lewis Jr., and M. G. Hayden (2002),
583 Effects of groundwater flux on open-channel estimates of stream metabolism, *Limnology*
584 *and Oceanography, 47*, 321-324.

585 Moran, P. A. P. (1950), Notes on Continuous Stochastic Phenomena, *Biometrika, 37*, 17-
586 23.

587 Mulholland, P. J. et al. (2001), Inter-biome comparison of factors controlling stream
588 metabolism, *Freshwater Biology, 46*, 1503-1517.

589 Neale, P. J. and J. Marra (1985), Short-term variation of P_{max} under natural irradiance
590 conditions - a model and its implications, *Mar. Ecol. Prog. Ser., 26*, 113-124.

591 Odum, H. T. (1956), Primary production in flowing waters, *Limnol. Oceanogr., 1*, 102-
592 117.

593 Oliver, R. L. and C. J. Merrick (2006), Partitioning of river metabolism identifies
594 phytoplankton as a major contributor in the regulated Murray River (Australia),
595 *Freshwat. Biol., 51*, 1131-1148.

596 Pahl-Wostl, C. and D. M. Imboden (1990), DYPHORA - a dynamic model for the rate of
597 photosynthesis of Algae, *J. Plankton Res., 12*, 1207-1221.

598 Reid, M. A., M. C. Thoms, and F. J. Dyer (2006), Effects of spatial and temporal
599 variation in hydraulic conditions on metabolism in cobble biofilm communities in an
600 Australian upland stream, *J. N. Am. Benthol. Soc., 25*, 756-767.

601 Rutherford, J. C. (1994), Transverse mixing, in *River Mixing*, pp. 95-173, John Wiley and
602 Sons Ltd, West Sussex, England.

603 Sand-Jensen, K. and P. A. Staehr (2007), Scaling of pelagic metabolism to size, trophy
604 and forest cover in small Danish lakes, *Ecosystems, 10*, 127-141.

605 Stillwater Sciences (2002), Merced River corridor restoration plan, 245.

606 Thyssen, N., M. Erlandsen, E. Jeppesen, and C. Ursin (1987), Reaeration of oxygen in
607 shallow, macrophyte rich streams: I - Determination of the reaeration rate coefficient, *Int.*
608 *Revue ges. Hydrobiol., 72*, 405-429.

609 Tsivoglou, E. C. and L. A. Neal (1976), Tracer measurement of reaeration: III. Predicting
610 the reaeration capacity of inland streams, *Journal (Water Pollution Control Federation),*
611 *48*, pp. 2669-2689.

612 Vadeboncoeur, Y., G. Peterson, M. J. Vander Zanden, and J. Kalff (2008), Benthic algal
613 production across lake size gradients: Interactions among morphometry, nutrients, and
614 light, *Ecology, 89*, 2542-2552.

615 Van de Bogert, Matthew C., D. L. Bade, S. R. Carpenter, J. J. Cole, M. L. Pace, P. C.
616 Hanson, and O. C. Langman (2012), Spatial heterogeneity strongly affects estimates of
617 ecosystem metabolism in two north temperate lakes, *Limnol. Oceanogr., 57*, 1689-1700.

618 Van de Bogert, Matthew C., S. R. Carpenter, J. J. Cole, and M. L. Pace (2007), Assessing
619 pelagic and benthic metabolism using free water measurements, *Limnol. Oceanogr.*
620 *Meth., 5*, 145-155.

621 Von Schiller, D., E. Marti, J. L. Riera, M. Ribot, J. C. Marks, and F. Sabater (2008),
622 Influence of land use on stream ecosystem function in a Mediterranean catchment,
623 *Freshwat. Biol., 53*, 2600-2612.

624 Wartenberg, D. (1985), Multivariate spatial correlation - a method for exploratory
625 geographical analysis, *Geogr. Anal., 17*.

626 Wilcock, R. J., P. D. Champion, J. W. Nagels, and G. F. Croker (1999), The influence of
627 aquatic macrophytes on the hydraulic and physico-chemical properties of a New Zealand
628 lowland stream, *Hydrobiologia, 416*, 203-214.

629 Wilcock, R. J., J. W. Nagels, G. B. McBride, K. J. Collier, B. T. Wilson, and B. A. Huser
630 (1998), Characterization of lowland streams using a single-station diurnal curve analysis
631 model with continuous monitoring data for dissolved oxygen and temperature, *N. Z. J.*
632 *Mar. Freshwat. Res., 32*, 67-79.

633 Wilcock, R. J. (1982), Simple predictive equations for calculating stream reaeration rate
634 coefficients, *New Zealand Journal of Science, 25*, 53-56.

635 Wilcock, R. J. (1988), Study of river reaeration at different flow-rates, *Journal of*
636 *Environmental Engineering-Asce, 114*, 91-105.

637 Zamora, C. (2007), Estimating water fluxes across the sediment-water interface in the
638 lower Merced River, California, *2007-5216*.

639

640 Table 1

	FIXED SYSTEM	
	Spring of 2009	Summer of 2009
Start	20/04/2009 14:11	07/09/2009 12:00
End	25/04/2009 09:58	12/09/2009 01:00
Sampling strategy	Continuous at 5-min intervals	Continuous at 10-min intervals
Data collected	Temp, DO, PAR	Temp, DO, PAR
Diel cycles	4 (days 1 through 4)	4 (days 1 through 4)
	MOBILE SYSTEM	
	Spring of 2009	Summer of 2009
Start	21/04/2009 10:26	07/09/2009 18:31
End	25/04/2009 10:10	12/09/2009 04:56
Sampling strategy	Raster plan, 11 locations, 93 cycles at variable intervals	Raster plan, 10 locations, 114 cycles at variable intervals
Data collected	Temp, DO, Chl, Vel	Temp, DO, Chl, Vel
Complete diel cycles	3 (days 2 through 4)	4 (days 1 through 4)

641 Table 2

Merced River – Stationary Metabolism Results					
			Areal rates (gr O_2 m^{-2} day^{-1})		
04/2009		$K_{2,20}$ (day^{-1})	CR_{24}	*GPP*	*NEP*
21	day 1	1.97±0.09	4.16±0.00	3.59±0.02	-0.57±0.02
22	day 2	2.02±0.05	4.29±0.00	3.64±0.02	-0.64±0.02
23	day 3	1.93±0.09	4.06±0.00	3.54±0.03	-0.51±0.03
24	day 4	1.97±0.05	3.61±0.00	2.77±0.02	-0.83±0.02
09/2009		$K_{2,20}$ (day^{-1})	CR_{24}	*GPP*	*NEP*
08	day 1	1.58±0.05	3.18±0.00	2.44±0.01	-0.73±0.01
09	day 2	1.46±0.05	3.23±0.00	2.52±0.01	-0.71±0.01
10	day 3	1.45±0.04	3.30±0.00	2.64±0.01	-0.67±0.01
11	day 4	1.49±0.07	3.21±0.00	2.47±0.01	-0.74±0.01

642 **List of Figures**

643 **Figure 1. Study site. Satellite image of the Merced River reach under investigation (source:**
644 **Google Earth) with water flowing from north-east to south-west.**

645 **Figure 2. Photograph of the experimental set up. (A) mobile sampling unit (water quality**
646 **and velocity); (B) fixed sampling unit (water quality and PAR); (WS) weather station; (L-1,**
647 **L-2, L-3) light intensity sensors. The image captures the predominant shading pattern along**
648 **the left bank of the river.**

649 **Figure 3. Example of the interpolation scheme for water temperature (top) and dissolved**
650 **oxygen (bottom) for the April data set. The continuous (grey) line represents the fixed-**
651 **station data and the symbols and black line represent the observations and 1-min spline-**
652 **interpolation, respectively, for the nearest sampling point (x = 9.5 m) of the distributed data**
653 **set.**

654 **Figure 4. Profiles of daily-average velocities across the river transect during April (top) and**
655 **September (bottom). Dashed lines with symbols represent velocities for day 1 (grey**
656 **diamond – September only), day 2 (black circles), day 3 (open triangles), and day 4 (gray**
657 **squares). The gray circular symbols indicate the position of the sampling points for the**
658 **distributed system [vertical scale exaggerated].**

659 **Figure 5. Time series of (a) air temperature, (b, c) solar radiation on-site and CIMIS**
660 **weather station, and (d) PAR at the experimental site (black line: April data; grey line:**
661 **September data).**

Figure 6. Incident light patterns at the study site represented by the normalized light intensity for three different positions across the river transect. (Top: April 21-24; bottom: September 08-11). The observations (lux) were normalized by the maximum observed value for the two experiments (200,000 lux).

Figure 7. Temperature (Temp), dissolved oxygen (DO) and chlorophyll-*a* (Chl), spatiotemporal behavior observed using the mobile sensor platform. For each panel, the horizontal axis represents position within a raster scan from the right to the left river bank (downstream look), the vertical axis represents the average sampling time for each raster scan (intervals are not uniform), and the colored cells represent the value of each sampled parameter (DO, Temp, Chl) for the corresponding position and time (note differences in scale).

Figure 8. Time series of the calculated Moran's *I* statistic for the two experiment periods. Black symbols refer to the April results and grey symbols to those of September. The filled dots indicate the transect runs for which significant ($p<0.05$) gradients were identified by the Moran's *I* statistic. For April, out of the 90 transects collected between days 1 and 4, there were 81 (Temp), 67 (DO), and 62 (Chl) transects in which Moran's *I* was significant. For September, 100 (Temp), 77 (DO), and 54 (Chl) out of 105 transects had significant Moran's *I*.

Figure 9. Time series of the normalized distribution of the coefficients of variation (*CV*) of the measured DO concentrations, for the April (top) and September (bottom) raw data. Each symbol represents the variability of one raster scan.

Figure 10. Representative morning and afternoon raster scans showing the spatial distribution of raw temperature (a), DO (b) and chlorophyll-*a* (c) data for April (left) and September (right). The figure shows the deviation of the measured value at each sampling point with respect to the average for the raster scan.

Figure 11. River cross-sectional distributions for (a) *GPP*, (b) CR_{24}, (c) *NEP*, and (d) *P/R* ratios for April (left) and September (right). All results are normalized with respect to the estimates obtained at point 10 (thalweg position) of the sampling transect (The error bars are based on the propagation of velocity and depth uncertainty through the reaeration and metabolism calculations).

692

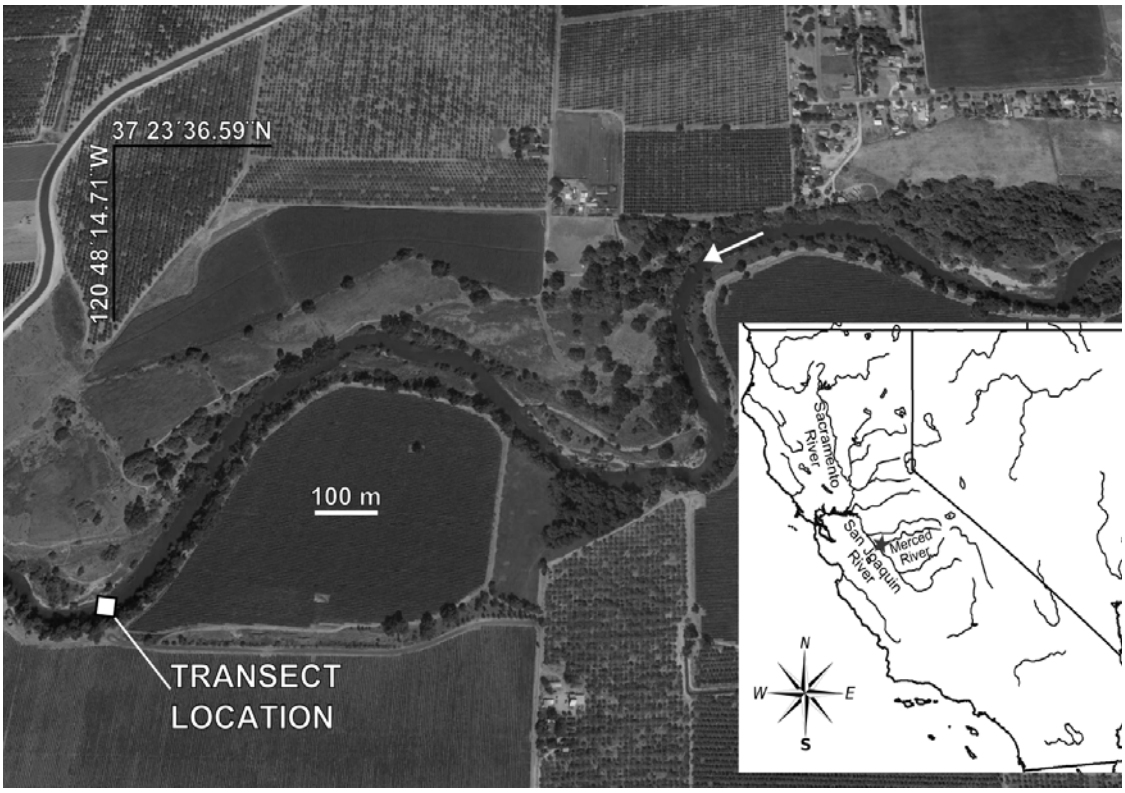

Figure 12. Satellite image of the Merced River study reach (source: Google Earth) with sampling transect location and approximate channel delineation.

693

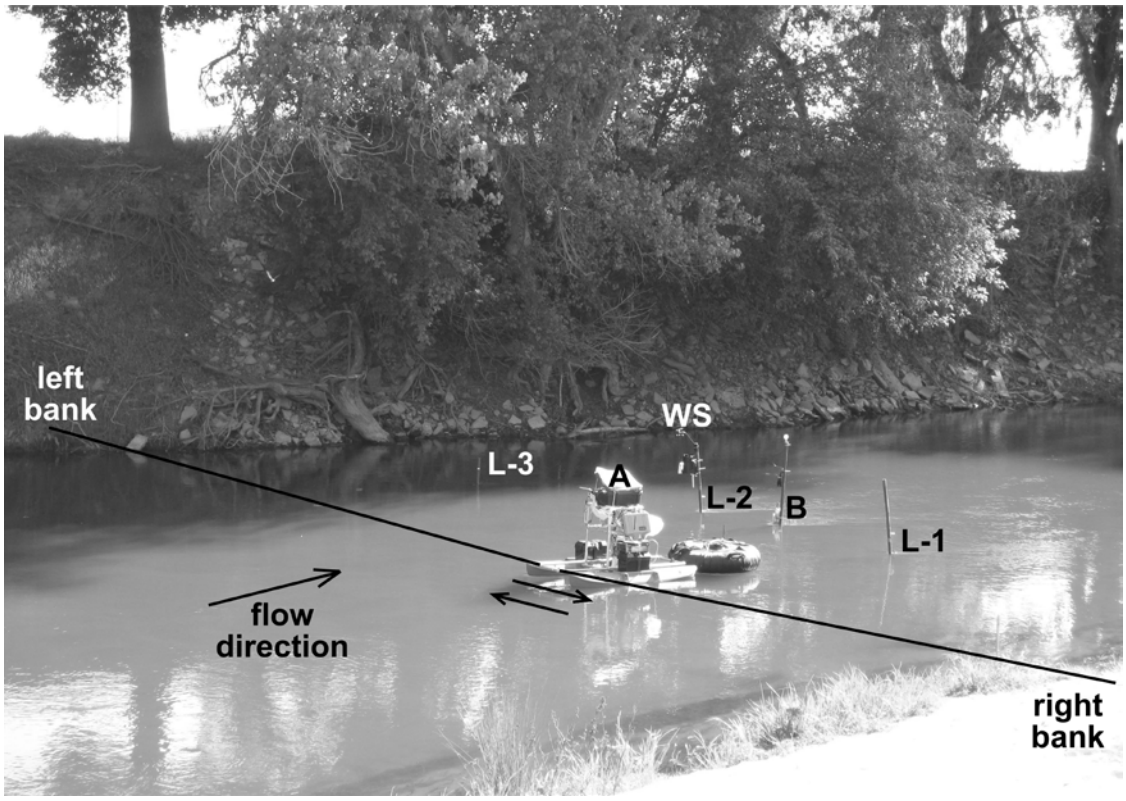

Figure 13. Photograph of the experimental set up. (A) mobile sampling unit (water quality and velocity); (B) fixed sampling unit (water quality and PAR); (WS) weather station; (L-1, L-2, L-3) light intensity sensors. The image captures the predominant shading pattern along the left bank of the river.

694

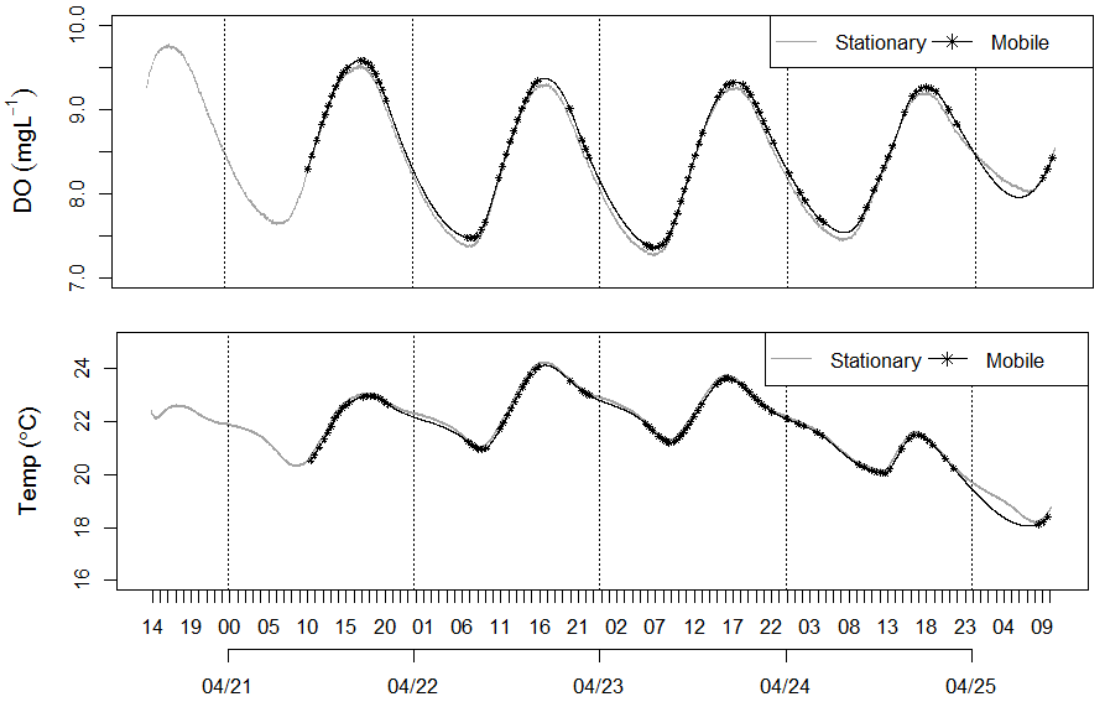

Figure 14. Example of the interpolation scheme for water temperature (bottom) and dissolved oxygen (top) for the April data set. The continuous (grey) line represents the fixed-station data for comparison, and the symbols and black line represent the observations and 1-min spline-interpolation, respectively, for the nearest sampling point (x = 9.5 m) of the distributed data set.

695

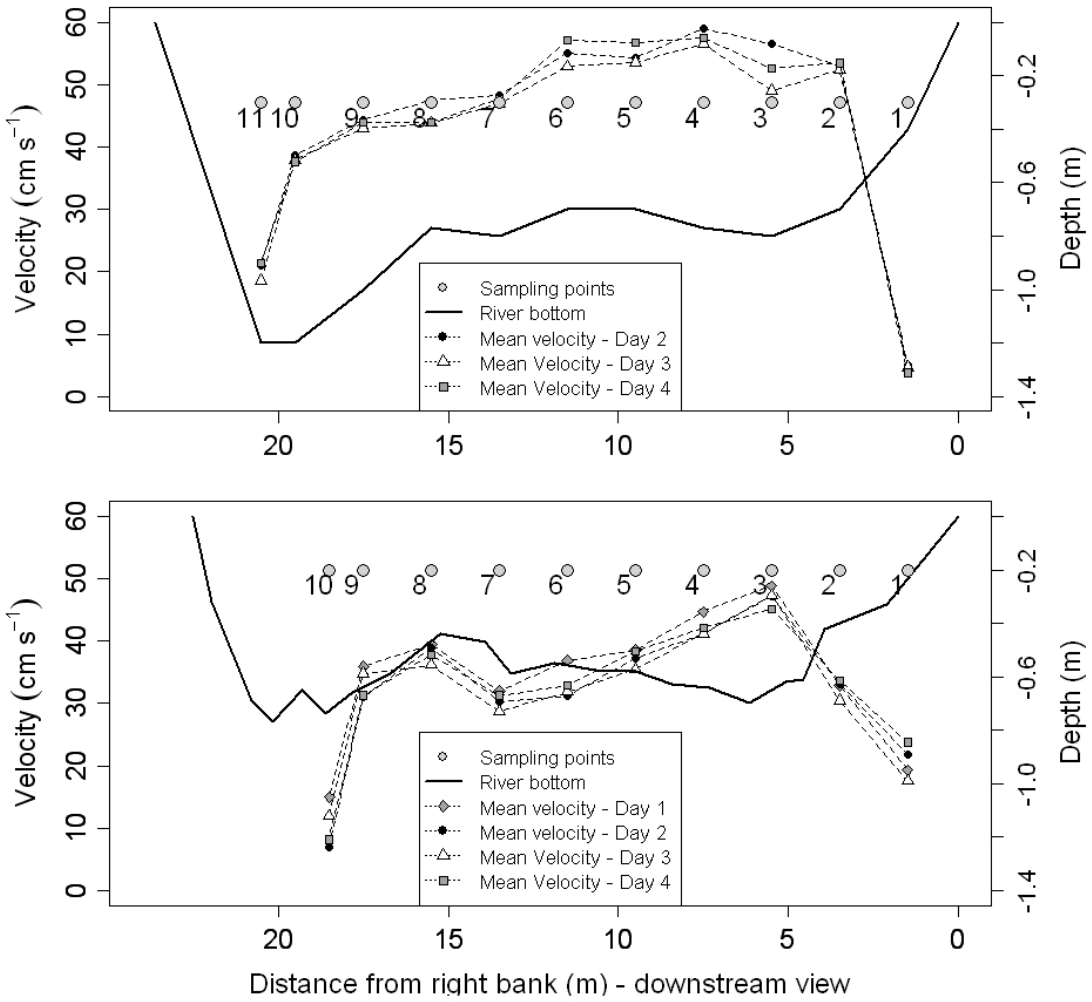

Figure 15. Profiles of daily-average velocities across the river transect during April (top) and September (bottom). Dashed lines with symbols represent velocities for day 1 (diamonds – September only), day 2 (black circles), day 3 (triangles), and day 4 (squares). The gray circles indicate the position of the sampling points for the distributed system [vertical scale exaggerated].

696

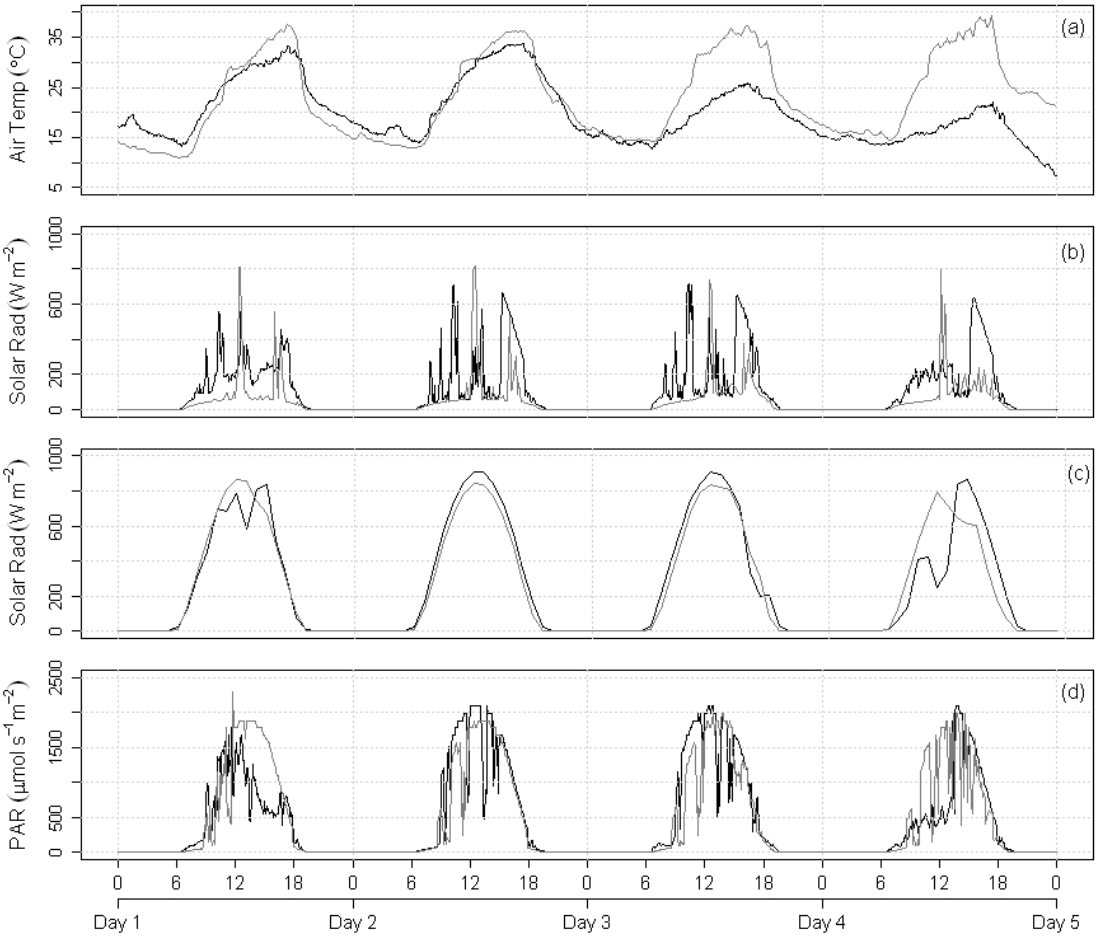

Figure 16. Time series of (a) air temperature, (b, c) solar radiation on-site and CIMIS weather station, and (f) PAR at the experimental site (black line: April data; gray line: September data).

697

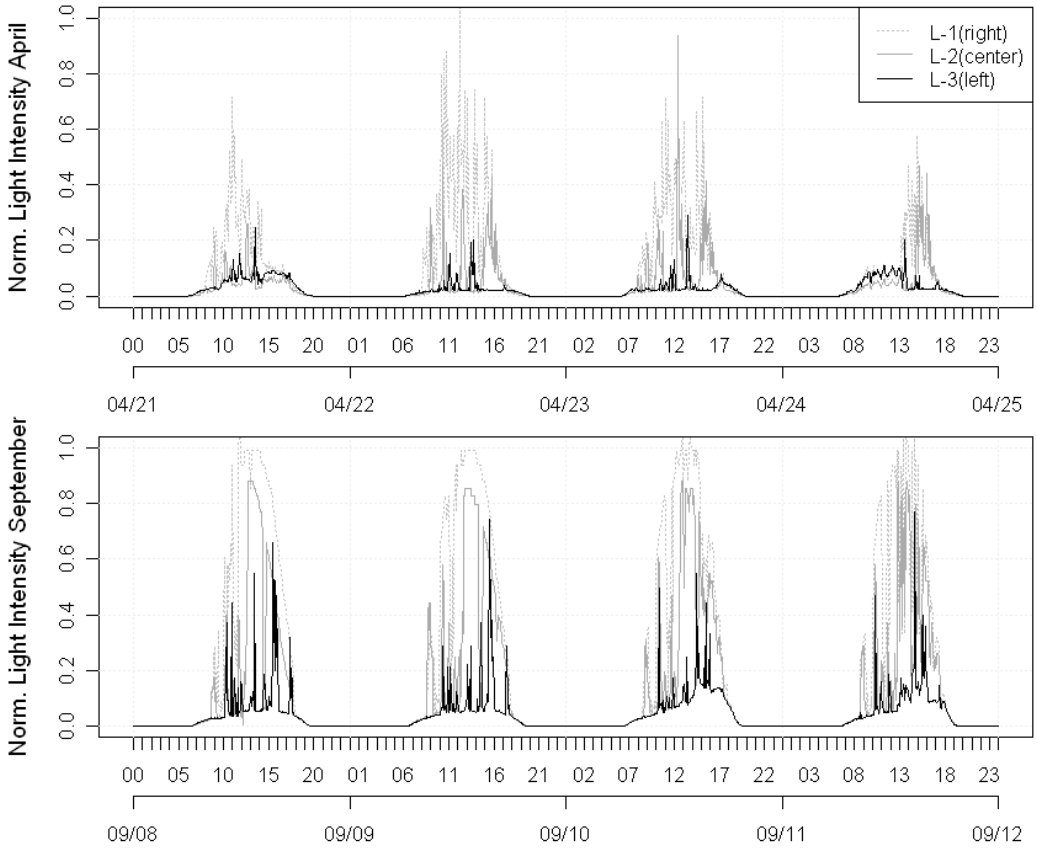

Figure 17. Incident light patterns represented by the normalized light intensity for three different positions across the river transect. (Top: April 21-24; bottom: September 08-11). The observations (lux) were normalized by the maximum observed value for the two experiments (200,000 lux).

698

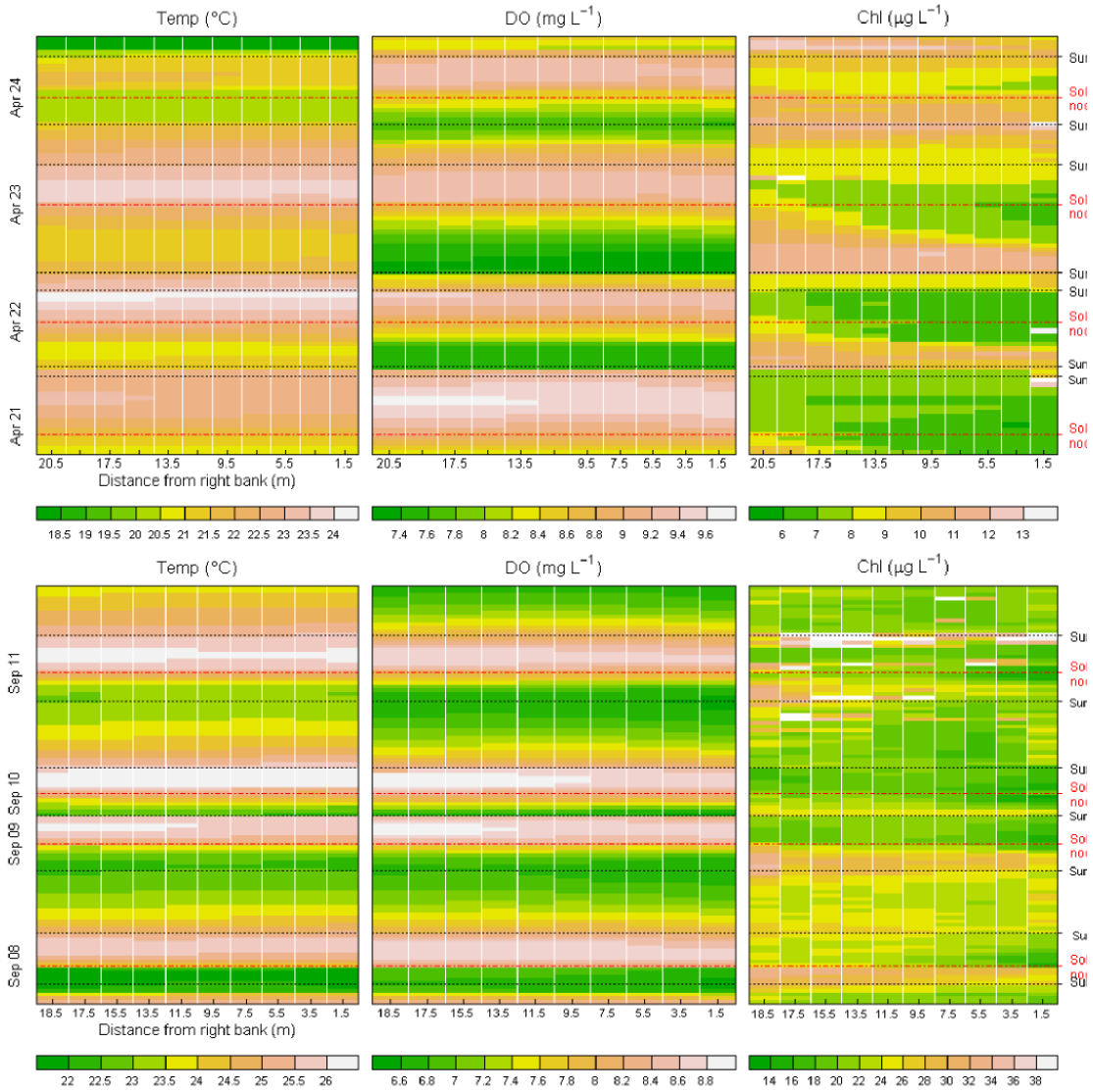

Figure 18. Temperature, dissolved oxygen (DO) and chlorophyll-*a* (Chl), spatiotemporal behavior observed using the mobile sensor platform. For each panel, the horizontal axis represents position within a raster scan from the right to the left river bank (downstream view), the vertical axis represents the average sampling time for each raster scan (intervals are nonuniform in time), and the colored cells represent the value of each sampled parameter (DO, Temp, Chl) for the corresponding position and time (note differences in scale).

699

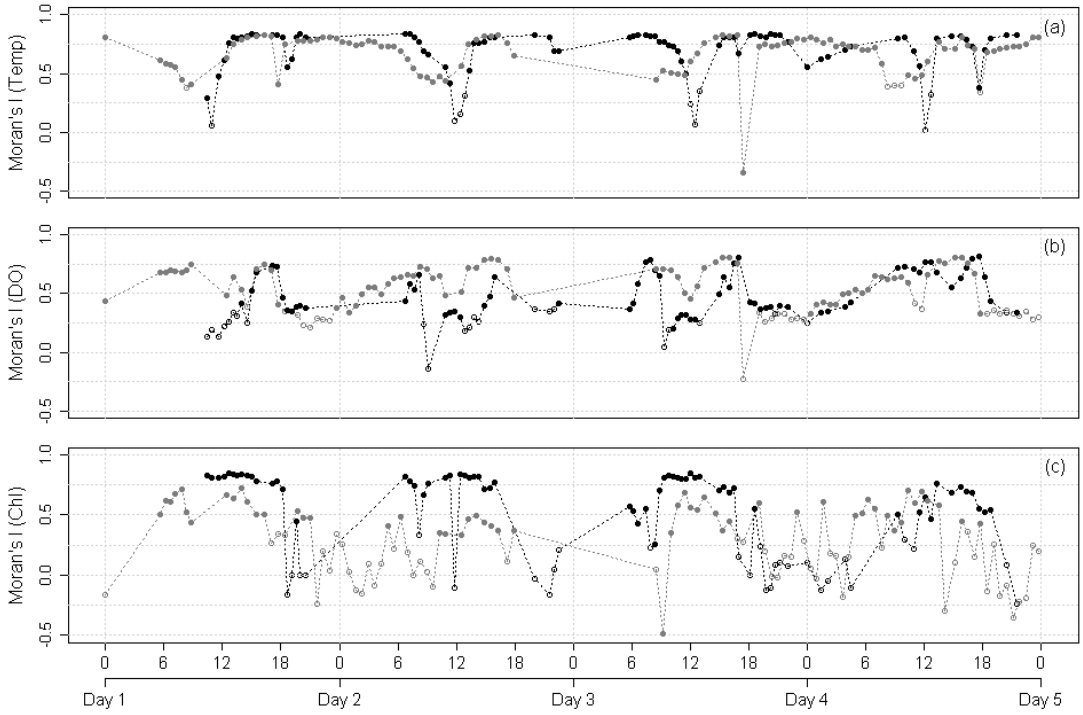

Figure 19. Time series of the calculated Moran's *I* statistic for all cross-sectional sampling events during the two experiment periods. Black symbols refer to the April results and gray symbols to those of September (solid symbols denote sampling events with statistically significant patterns, $p < 0.05$).

700

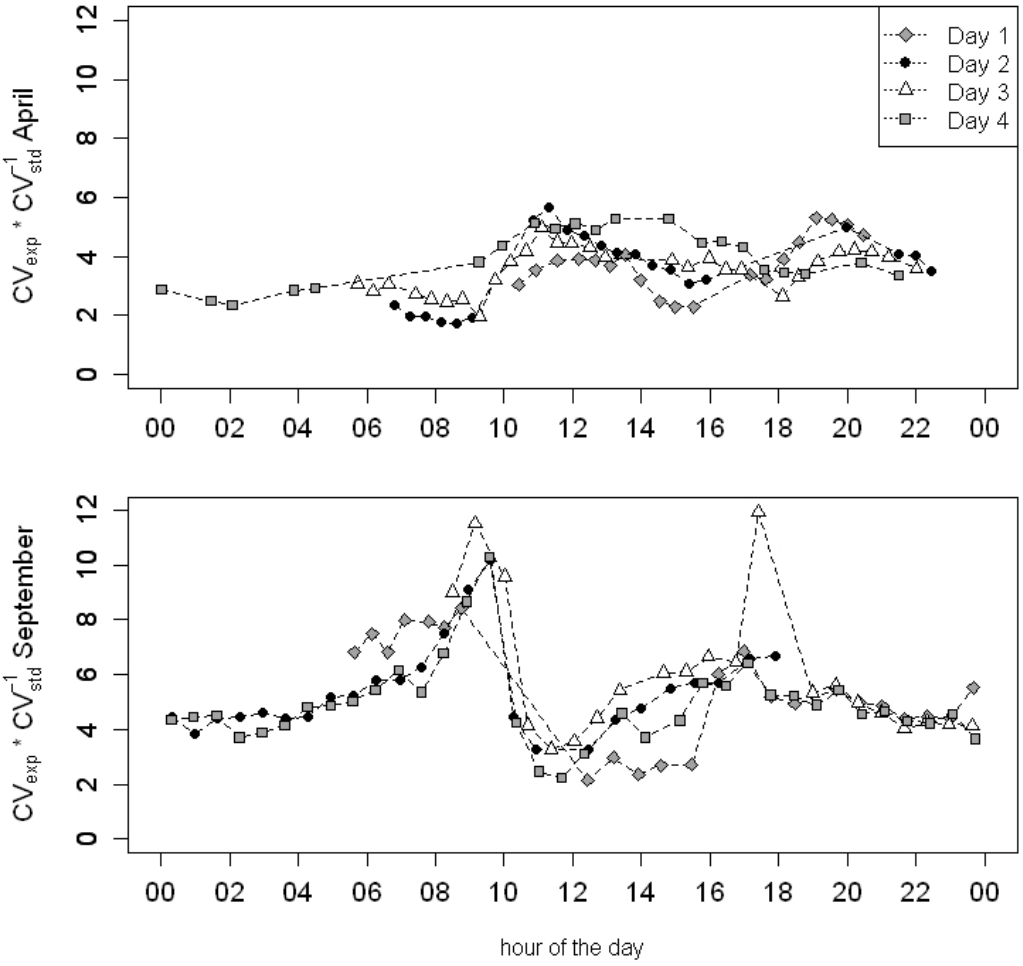

Figure 20. Time series for April (top) and September (bottom) normalized coefficients of variation (*CV*) for spatially distributed DO concentrations at the time shown (each symbol represents the variability of one cross-sectional sampling event).

701

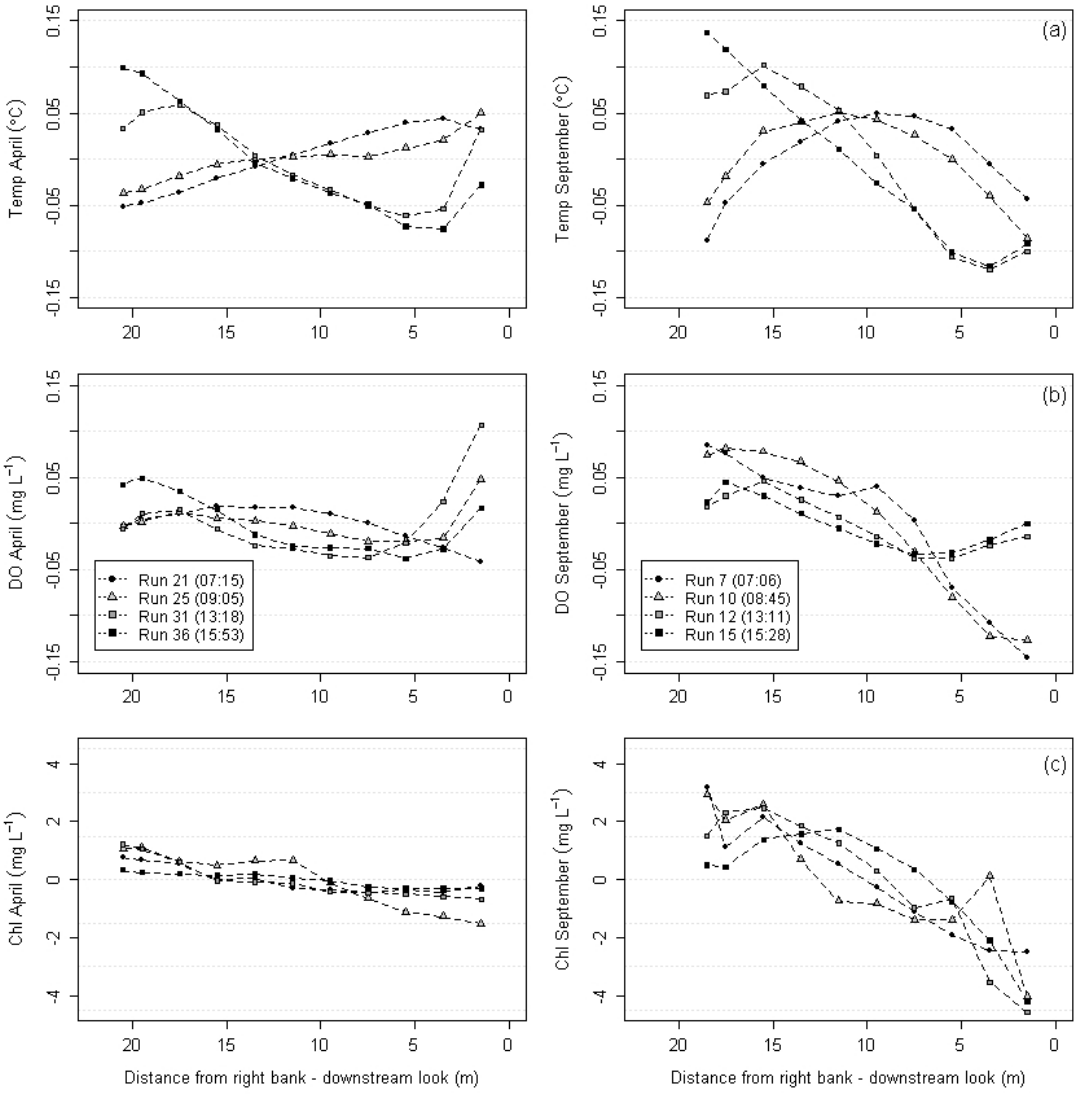

Figure 21. Deviation of local (a) temperature, (b) DO and (c) chlorophyll-a measuremetns from the cross-sectional average for selected morning and afternoon sampling events in April (left) and September (right).

702

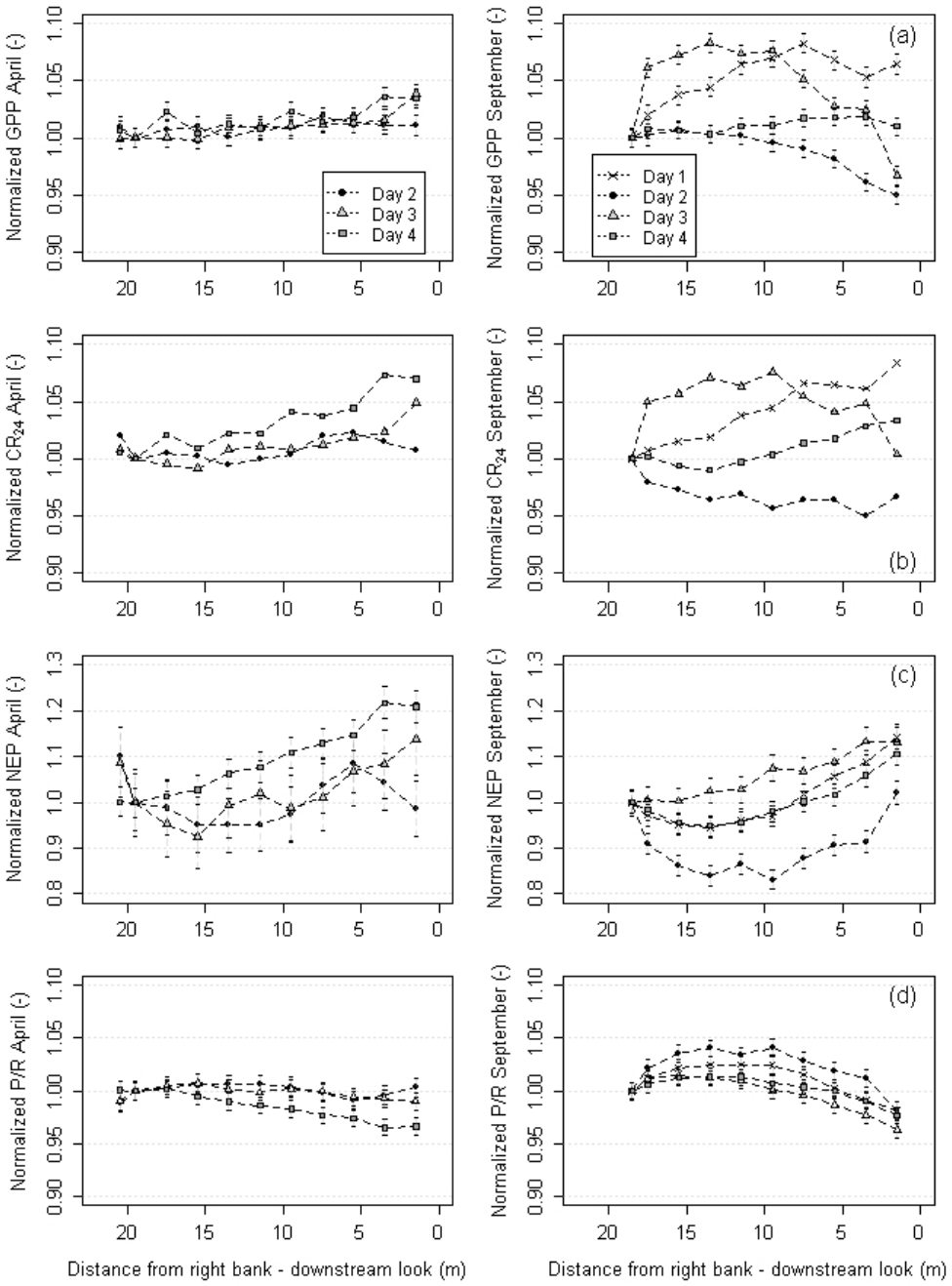

Figure 22. River cross-sectional distributions for (a) *GPP*, (b) CR_{24}, (c) *NEP*, and (d) *P/R* ratios for April (left) and September (right); values are normalized with respect to the thalweg sampling position (point 10). Error bars are based on the propagation of velocity and depth uncertainty through the reaeration and metabolism calculations.

703

704